

Many-body localization in long range hopping model: Real space renormalization group study

Ranjan Modak¹ and Tanay Nag²

¹ *SISSA and INFN, via Bonomea 265, 34136 Trieste, Italy and*

² *SISSA, via Bonomea 265, 34136 Trieste, Italy*

We develop a real space renormalization group (RSRG) scheme by appropriately inserting the long range hopping $t \sim r^{-\alpha}$ with nearest neighbour interaction to study the entanglement entropy and maximum block size for many-body localization (MBL) transition. We show that for $\alpha < 2$ there exists a localization transition with renormalized disorder that depends logarithmically on the finite size of the system. The transition observed for $\alpha > 2$ does not need a rescaling in disorder strength. Most importantly, we find that even though the MBL transition for $\alpha > 2$ falls in the same universality class as that of the short-range models, while transition for $\alpha < 2$ belongs to a different universality class. Due to the intrinsic nature of the RSRG flow towards delocalization, MBL phase for $\alpha > 2$ might suffer an instability in the thermodynamic limit while the underlying systems support algebraic localization. Moreover, we verify these findings by inserting microscopic details to the RSRG scheme where we additionally find a more appropriate rescaling function for disorder strength; we indeed uncover a power law scaling with a logarithmic correction and a distinctly different stretched exponential scaling for $\alpha < 2$ and $\alpha > 2$, respectively, by analyzing system with finite size. This finding further suggests that microscopic RSRG scheme is able to give a hint of instability of the MBL phase for $\alpha > 2$ even considering systems of finite size.

I. INTRODUCTION

Localization-delocalization transition occurring in quantum system separates the non-ergodic, reversible phase from the ergodic, irreversible phase of matter^{1,2}. The concept of Anderson localization, observed in single particle picture³, can be elevated to many-body localization (MBL) in the interacting system even in finite temperature^{4,5}. The intensive investigation of the above phenomenon unfolds many unusual response properties^{6,7}, new nature of quantum entanglement⁸⁻¹⁰, and non-trivial phases of matter absent in equilibrium¹¹. For example, MBL phase violates eigenstate thermalization hypothesis (ETH)¹²⁻¹⁶, is characterized by an area law of entanglement entropy (EE) and localization length, while delocalized ergodic phase satisfies volume law for both of them^{17,18}. On the other hand, in the context of time periodic Floquet system, MBL phase can help in exploring the Floquet time crystal^{19,20}. Cold atomic systems happen to be a good test bed for investigating the MBL transition^{21,22}. The experimental search has already began in this field of research to check the theoretical predictions^{23,24}. However, it is important to point out that even though analytic perturbative arguments support the existence of MBL^{25,26}, very recently the stability of this phase has been questioned in interacting systems with correlated²⁷ and un-correlated disorder²⁸.

It is natural question to ask that whether MBL transition persists for long range hopping: $t \sim r^{-\alpha}$ as Anderson showed that single particle localization can not occur in the presence of long range hopping for $\alpha \leq d$ where d is the dimension of the system. Most of the numerical attempts in one dimensional system show that MBL can not survive for $\alpha < 2$ while MBL occurs for $\alpha > 2$ ²⁹⁻³². Interestingly, perturbative treatment on an effective An-

derson model can show MBL transition even for $\alpha < 1$ ³³. Recently, it has been found that a different kind of localization namely, algebraic localization, takes place due to the presence of long-range hopping^{34,35}, which gives rise to some interesting unique phenomena such as anomalous transport^{36,37} and a sub-extensive scaling of EE³⁸. Moreover, in the context of quantum spin chain the long range interaction is also investigated in detail leading to a plethora of non-trivial results³⁹⁻⁴¹. These upsurge of theoretical studies in long range model are highly motivated by a series of earlier experimental investigations⁴²⁻⁴⁸.

In the context of MBL transition, a promising alternative to the existing exact diagonalization(ED) technique is real space renormalization group (RSRG) description⁴⁹⁻⁵⁴. The main advantage of using the RSRG technique is that it can overcome the system size limitation. Within this approach, we solve a macroscopic version of the underlying model instead of solving the actual interacting microscopic model where the Hilbert space dimension grows exponentially with system size. The common principle employed in all the RG schemes is that the collective resonant tunneling processes are energetically favored in the delocalized phase while localized phase supports the formation isolated islands caused by the suppression of resonant tunneling. Moreover, there has been a recent proposal to incorporate the microscopic details in the RSRG scheme to study models with quasi-periodic potential⁵⁵. Till now all ED results suggests the violation of Harris-Chayes-Chayes-Fisher-Spencer criterion^{56,57}, which claims the diverging localization length exponent $\nu \geq 2/d$. Interestingly, ν obtained from RSRG studies satisfies the above criteria.

Much having explored in the field of RSRG technique with the short range hopping model, our focus here is to extend the RSRG analysis to the interacting long range system with hopping as $t \sim r^{-\alpha}$. The questions that

we would like to answer are how one can identify and characterize the MBL transition in long range hopping system with α in presence of nearest neighbor interaction. Overcoming the system size barrier that one encounters in ED, RSRG formalism can decisively convey that the renormalization of disorder strength is essential to observe the true MBL transition in the thermodynamic limit for this kind of system with $\alpha < 2$. On the contrary, MBL transition for $\alpha > 2$ requires no renormalization of disorder strength. Most interestingly, our analysis with correlation length exponent ν suggests that the universality class of the MBL transition occurring for $\alpha < 2$ is different than the usual Anderson type which we observe for $\alpha > 2$. We then strengthen our findings by incorporating the microscopic details in the RSRG scheme where we additionally find a more appropriate renormalization of disorder strength. We here find that our numerically obtained scaling functions for the disorder strength are mostly in congruence with analytical studies considering long range nature of hopping as well as interaction^{29,58}. The microscopic RSRG scheme allows us to get a hint about the instability of the MBL phase for $\alpha > 2$ even with the finite size of the system where macroscopic RSRG predicts a MBL transition. It would be an interesting question to study the stability of MBL transition for $\alpha > 2$ in algebraic localization considering large system size.

We shall now discuss about the organization of the paper. We first introduce the RSRG algorithm for the long range system in Sec. II. We also present the prescription for the calculation of EE and MBS. We then elaborate on our findings in Sec. III. We here analyze the behavior of EE and MBS to characterize the MBL transition occurring in finite size system. Next, we briefly discuss the microscopic input to this RSRG scheme and investigate its consequences. We compare microscopic and macroscopic RSRG findings by analyzing the histogram of largest blocks in Sec. IV. Lastly, in Sec. V, we conclude.

II. RG SCHEME

We now describe in details the implementation of the RSRG approach, which we employ here to study the long-range models. The main idea is to investigate the structure of resonance clusters, caused by the destabilization of MBL phase, using appropriate RG rules for our systems. Finding all such generic many-body resonances for a microscopic models is a challenging problem both analytically and also even numerically. Numerical studies suffer from severe system size limitations, because of the exponential growth of Hilbert space dimension with system size L . Hence, instead of solving the full resonance structure for any such microscopic Hamiltonian, we first identify small resonant clusters starting from two-sites resonance pairs. We then examine whether groups of these small resonant clusters can collectively resonate or not. We apply these techniques iteratively to identify the

the structure of resonance clusters in the large scale. The RG rules with technical detail, which is very similar to the one proposed by Dumitrescu et al.⁵⁴, are described below. We at the same time note that RSRG approach can be regarded as a certain toy model for MBL transition, whether or not the RSRG rules provide a correct description of MBL transition is still a subject of debate. The ED provides a full grasp into complex nature of disordered interacting systems which might not be fully captured by RSRG schemes.

We note that the RSRG approach is not limited to a certain type of lattice model. However, one can think a corresponding microscopic model

$$H = - \sum_{i,j \neq i} J_{ij} (\hat{c}_i^\dagger \hat{c}_j + \text{H.c.}) + \sum_i \mu_i \hat{n}_i + V \hat{n}_i \hat{n}_{i+1} \quad (1)$$

where \hat{c}_i^\dagger (\hat{c}_i) is the fermionic creation (annihilation) operator at site i , $\hat{n}_i = \hat{c}_i^\dagger \hat{c}_i$ is the number operator. μ_i is the chemical potential uniformly distributed on the interval $[0, W]$. $V \ll (J_{ij}, W)$ is the strength of nearest neighbour interaction. J_{ij} is considered to be the long-range hopping between i and j -th site leading to the algebraically localized SPSs. L is the size of the system. It is noteworthy that once $J_{ij} = J_{i,i+1} = J$, being restricted to the nearest neighbour only, the i -th SPS is exponentially localized near site i with energy $\epsilon_i \simeq \mu_i + \mathcal{O}(J^2/W)$. In the case of nearest-neighbour interaction only, the diagonal energy mismatch is simply given by $\Delta E_{ij} = |\epsilon_i - \epsilon_j| \sim |\mu_i - \mu_j|$. Then the idea of the RSRG scheme is to consider the nearest neighbor interaction V as a perturbation and express the tunneling in terms of SPSs which are exponentially localized in the above case. Hence, the tunneling amplitude is having the form $\Gamma_{ij} = V \exp(-|i - j|/x_0)$ with x_0 be the localization length⁵⁰. We would like to mention that for the long-range interacting case²⁹ with $V_{ij} \hat{n}_i \hat{n}_j$, the energy mismatch between two sites i and j becomes $\Delta E_{ij} \sim |\mu_i - \mu_j + \sum_{k \neq i,j} (V_{ik} - V_{jk}) \hat{n}_k|$. In general, the role of interactions is to set in the multi-particle collective resonances. For weak interactions, the system remains in MBL phase and the local integrals of motion associated with the weakly dressed single-particle orbitals become few-body local integrals of motion²⁵. For strong enough interactions, MBL phase breaks down as the clusters become resonantly linked.

Given these details, we shall now implement the RSRG scheme with long-range hopping J_{ij} while the interaction V is considered to be nearest neighbour. At the outset, we discuss the main philosophy behind our RSRG scheme that we adopt. For very strong disorder, the resonantly linked pairs are well separated and their density is very small. As the disorder weakened, these resonant links are more frequently formed eventually leading towards the disruption of localization. One can note that the process of making the collective resonant links has to be energetically favored. These could lead to an avalanche

mechanism where the system continues to stuck and the size of the resonant cluster grows^{58,59}. Therefore, the delocalization stems from the these avalanches. Below we shall discuss it with technical detail.

First, we consider a chain of L sites and assign each sites with some random number $\lambda_i = [0, W]$ identified as on-site energy. Next, we need to initialize the tunneling matrix elements Γ_{ij} , which represent the typical tunneling amplitude between i and j sites. As the single-particle wave-function of long-range models are found to be algebraically localized instead of exponential, we choose $\Gamma_{ij} = V/|i-j|^\alpha$, being our initial values. Here V can be thought of the nearest neighbor interaction strength; we set $V = 0.5$ for all our calculations. Then, we start our RG procedure by comparing the tunneling matrix elements Γ_{ij} between sites i and j with the energy mismatch $\Delta E_{ij} = |\lambda_i - \lambda_j|$. If $\Gamma_{ij} > \Delta E_{ij}$, we merge those sites to build a cluster. We continue this process iteratively. In each step, Γ and ΔE are modified as, $\lambda_{i'} = [\sum_i \lambda_i^2 + \sum_{ij} \Gamma_{ij}^2]^{1/2}$, $\delta_{i'} = \lambda_{i'}/(2^{n_{i'}} - 1)$, and $\Delta E_{i'j'} = \delta_{i'}\delta_{j'}/\min(\lambda_{i'}, \lambda_{j'})$, where i' and j' are newly formed clusters and $n_{i'}$ is the number of sites in cluster i' . There is an exception if $\lambda_{i'} \geq \delta_{i'} \geq \lambda_{j'} \geq \delta_{j'}$, we then consider $\Delta E_{i'j'} = \min(\delta_{i'} - \lambda_{j'}, \delta_{j'})$. The renormalization rules of Γ during the iterative process are chosen in the following way. If two clusters are not modified during a RG step, the coupling between them is set to zero and if at least one of the two clusters is modified during the RG step, Γ is given by,

$$\Gamma_{i'j'} = \left[\max_{i_1 \in \{i\}, i_2 \in \{j\}} \Gamma_{i_1 i_2} \right] e^{-(n_{i'} + n_{j'} - n_{i_1} - n_{i_2}) s_{\text{th}}/2}$$

where $s_{\text{th}} = \ln 2$ is the characteristic entropy per site in the thermal phase. This form is believed to be hold for matrix element of local operators that obey ETH⁵⁴. The RG iterative process terminates when no new resonant bond emerges, i.e. the cluster structure receives no modifications by further RG steps.

In this paper, we investigate two quantities. 1) Bipartite EE, obtained by dividing the system into two equal half. After the end of a RG procedure for a given initial disorder realization, the EE is technically defined as $S = \sum_C \min(m, n)$. The sum is over all the clusters which span the interval boundary and m, n are number of sites which are separated by the partition of the systems for such clusters. 2) Localization length ξ , which is defined by the maximum block size (MBS) found at the end of a RG procedure for a particular initial disorder realization. We run our RG procedure for $10^5 - 10^6$ times for different random realization to obtain average value of EE and MBS.⁵⁴ This technique allows us to simulate system size up to $L \simeq 500$ in contrast to the ED technique, which is practically impossible to implement for any size $L > 20$. We analyze the above quantities by varying the tunneling exponent α as defined in the RG nomenclature. However, considering the underlying physics behind α , one can understand that long range

(short range) corresponds to $\alpha < 2$ ($\alpha > 2$). However, we note that the convergence of our RSRG scheme is much slower compared to the RSRG scheme used previously for systems with exponentially localized SPSS⁵⁰. Hence, our numerical calculations are limited within the system size $L \sim \mathcal{O}(10^3)$.

As passing remarks, we would like to mention that the rules of the RSRG scheme imply a thermal cluster of size l_T can thermalize spins which are located at distance $R_{\text{AL}} < C 2^{l_T/a}$ from the core of the inclusion where C is a constant. The distance R_{AL} grows exponentially with the size l_T of the thermal inclusion and the probability of thermalizing the whole system by such a thermal inclusion quickly reaches 1 with increasing l_T . This means that the strong disorder phase is, in fact, not stable to inclusion of a sufficiently large thermal region when the size of the system is thermodynamically large $L \rightarrow \infty$. The uncorrelated nature of the disorder and algebraic structure of single particle states might be responsible for the above instability. At large W , the probability of occurrence of a thermal cluster of size l_T is very small and the strong disorder phase appears to be localized. However, the probability grows with system size L eventually leading to thermalization at any W . On the other hand, we would like to emphasize the difference in the RSRG for short-range systems where a thermal inclusion of size l_T thermalizes only spins residing within a fixed region R_{EL} that is related to the localization length of the system. Hence this size of R_{EL} would not grow with the system size $L \rightarrow \infty$.

III. RESULTS

We here shall describe the behavior of EE and MBS obtained using RSRG scheme described previously. We systemically study the critical behavior associated with the transition in Sec. III A and Sec. III B.

A. Macroscopic RSRG

Our aim is to probe the transition with disorder strength W by looking at the behavior of EE density S/L for different values of L . In fig. 1 (a) with $\alpha = 1.2$, we show S/L starts from unity for small W and gradually it falls with increasing W . $S/L \rightarrow 1(0)$, refers to the fact that the system is in a delocalized (localized) phase. We see that in the small W region, S/L falls more rapidly for smaller L than larger L while in the large W region, S/L saturates more quickly for smaller L . As a result, we see many intersections of S/L between different lengths. A careful analysis suggests that with increasing L , the intersection between two consecutive L shifts towards a higher value of W ; we refer $W = W_i$ where intersection occurs. One can demarcate the zone between maximum and minimum value of W_i as ΔW ; this is depicted by orange dashed line.

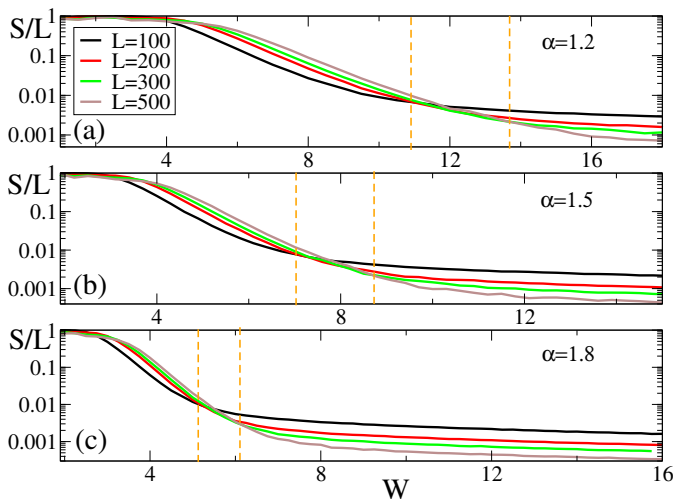


FIG. 1. (Color online) Plot shows the variation of entanglement entropy (EE) density S/L as a function of disorder strength W for three tunneling exponents $\alpha = 1.2$ in (a), $\alpha = 1.5$ in (b) and $\alpha = 1.8$ in (c) with $L = 100, 200, 300$ and 500 . The intersection point between two consecutive L shifts towards a higher values of W as one increases W . The orange dashed line represents the disorder window ΔW within which all the intersection are taking place. One can notice with increasing α , ΔW shrinks.

Another noticeable observation is that for $W \gg \max\{W_i\}$, S/L does not saturate to a constant value rather their saturation value increases with decreasing L . This phase is then no longer a delocalized phase. For finite size of the system, one can say that there is a delocalization-localization transition if one varies W from $W \ll \min\{W_i\}$ to $W \gg \max\{W_i\}$. Therefore, the existence of W_i refers towards a transition but the transition points becomes system size dependent. We repeat this investigation for $\alpha = 1.5$ (see Fig. 1 (b)) and $\alpha = 1.8$ (see Fig. 1 (c)) keeping $\alpha < 2$. We observe qualitatively similar feature of the transition but the width of ΔW shrinks and W_i 's shifts towards lower values.

We here discuss the uniqueness of this observation. This is in sharp contrast to the short range lattice models that support exponentially localized single particle states (SPSs)^{51,60}. For the above kind of model, one can observe a prominent transition point (designated by W_c) that does not change with L referring to the fact that the localization-delocalization transition is sharply defined in the finite size system. It is obviously stable in the thermodynamic limit. On the contrary, what we observe here in long range finite size system for $\alpha < 2$ can better be referred as a crossover. We note that the analogous microscopic long range Hamiltonian supports algebraically localized SPSs³⁴. Precisely, the intersection point W_i is size dependent hence, a conventional transition signature between two phases can not be assigned for finite L . The true existence of the localization-delocalization transition in thermodynamic limit $L \rightarrow \infty$ is therefore a subject of

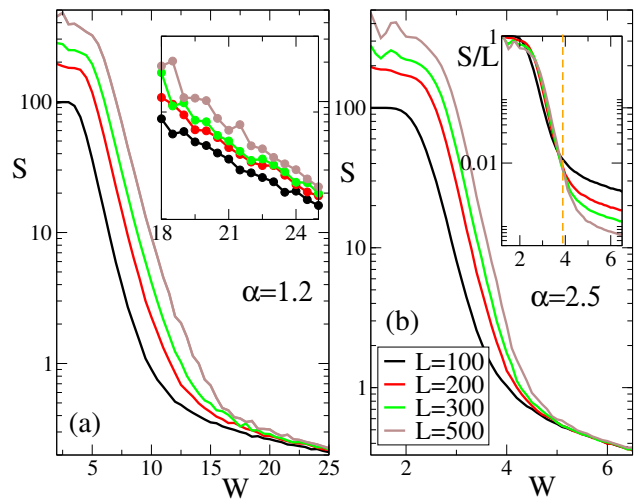


FIG. 2. (Color online) The plot depicts the variation of EE S as a function of W for $\alpha = 1.2$ in (a) and $\alpha = 2.5$ in (b). (a): One can observe that the system residing in delocalized phase ($S \sim L$) meets a transition at $W \simeq 20$ above which volume law of EE is no longer satisfied. Inset exhibits a zoomed in figure for $18 < W < 25$ where saturation characteristics of S still shows L dependence. (b): It shows a clear transition from delocalized to localized phase above $W > W_c = 3.95$ where EE satisfies a clear area law. The inset shows the variation of S/L with W where W_c is identified by the dashed orange line.

investigation which we shall present below.

Having discussed the situation with $\alpha < 2$, we shall now focus on $\alpha > 2$ sector. In this case, the system is expected to show similar behavior as compared to the short range models³¹. We compare the behavior of S between $\alpha = 1.2$ (see Fig. 2(a)) and $\alpha = 2.5$ (see Fig. 2(b)). For $\alpha = 1.2$ case, S for different L does not show any coincidence for larger values of W ; although, EE shows a tendency towards saturation where saturation value increases with increasing L (see the inset for Fig. 2(a) where a zoomed version of S is plotted for $18 < W < 25$). A clear distinction is seen in $\alpha = 2.5$ where S for all L coincides with each other for $W > W_c$. Once again We emphasize that for $\alpha = 2.5$, the inset of Fig. 2(b) depicts a sharp transition point W_c for all values of L similar to one observes for short-range models. While comparing with Fig. 1(a), it is clear that crossover occurs as W_i becomes a function of L .

One can hence infer that the nature of the phase transition even in finite size system changes from $\alpha < 2$ to $\alpha > 2$ as far as the saturation characteristics of S is concerned. The nature of phase transition for $\alpha > 2$ refers to the fact that EE obeys area law for $W > W_c$. On the other hand, for $\alpha < 2$, EE apparently follows a sub-extensive scaling violating the area law³⁸; this is a very unconventional outcome for a localized phase. Therefore, the natural question comes whether this saturation behavior is an artifact of the crossover.

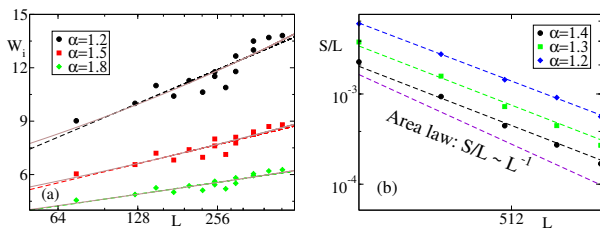


FIG. 3. (Color online) (a): We show the scaling of intersection points W_i (solid back, red and green points), obtained from crossing between different L , with L (in log scale) for $\alpha = 1, 2, 1.5$ and 1.8 . The dashed best fit straight lines show that $W_i \sim \gamma \ln L$ where γ depends on α . The brown solid lines represent the $L^\eta \ln L$ fitting of W_i where we find $\eta \ll (2 - \alpha)$; $\eta = 0.11, 0.08, 0.05$ for $\alpha = 1.2, 1.5, 1.8$. (b): We show the scaling of EE density, depicted by solid black, green and blue points, with L (in log scale) with $W = 20$ for $\alpha = 1, 2, 1.3$ and 1.4 . The dashed violet straight lines confirms the area law in the localized phase with $W^* = 3.0$.

Having compared S between $\alpha < 2$ and $\alpha > 2$, we turn our focus to investigate about the intersection point more extensively. One can notice that S/L for a given L intersects with all the other L (denoted by L') in many different positions as denoted by $W_i(L, L')$. The prescription that we are following is $W_i(L, L') \rightarrow W_i((L + L')/2) = W_i(L)$; as a result, we get a large set of data points which helps in describing the feature of W_i with L more precisely. We have also checked the robustness of our results by adopting different methods for identifying W_i e.g., geometric mean $W_i(L, L') \rightarrow W_i(\sqrt{LL'}) = W_i(L)$. These different scheme lead to the same scaling function of W_i as reported below. One can, on the other hand, choose $W_i(L, L + 100) \rightarrow W_i(L + 50) = W_i(L)$ as in our analysis we have $L = 100, 200, 300, 400, 500$. Figure 3(a) clearly suggests the intersecting points W_i logarithmically scales with L : $W_i \sim \gamma \ln L$ for $\alpha < 2$. However, the prefactor γ depends on α . However, we also examine the $L^\eta \ln L$ scaling of W_i ; the best fit value of η appears to be dependent on α , but $\eta \ll (2 - \alpha)$. Note that $\eta = 2 - \alpha$ has been predicted earlier in long-range interacting models^{29,58}. As far as the merit of the scaling is concerned, we check that our results remain unaltered within numerical accuracy considering both of the scaling function. Furthermore, unless L is chosen to be thermodynamically large, one really can not distinguish between these two scaling function. The power law scaling L^η might prevail for large L . Both of these scaling apparently prohibits the transition to happen in the thermodynamic limit: $L \rightarrow \infty$, $W_i \rightarrow \infty$. On the other hand, γ approaches zero as one approaches $\alpha = 2$; this conveys the fact that there exists a sharp transition point W_c which is independent of L . Hence, the transition obtained for $\alpha > 2$ is stable at least in finite system of size $L \sim O(10^2)$. In the thermodynamic limit $L \rightarrow \infty$, the stability of MBL phase might be obstructed as the length of the influence region R_{AL} grows with the length of the thermal block l_T (see Sec. II, for detail discussion).

We are now in a position to investigate the crossover phenomena. Instead of considering the bare W , we can continue our analysis with the renormalized W namely, W^* according to the numerically predicted scaling

$$W^* = \frac{W}{\gamma L^\eta \ln L}. \quad (2)$$

The motivation behind this renormalization is to identify the proper transition point W_c^* for a thermodynamic system. Figure 4(a) depicts the variation of S/L as a function of rescaled disorder W^* with $\alpha = 1.2$. There one can clearly notice the existence of a critical point W_c^* separating the delocalized phase from the localized phase. We shall extensively describe below this observation with plausible argument.

We now probe the saturation scaling of EE with L for a large but fixed value of W and W^* simultaneously. Figure 3(b) apparently suggests that for $\alpha < 2$, S/L scales as $L^{-\eta}$ with $\eta \simeq 0.9$ in the large $W > \max\{W_i\}$ limit as depicted by the solid point symbols. Even though, this observation is in congruence with the non-interacting case of the microscopic model³⁸, the scaling exponent however remains almost independent of the choice of α unlike the non-interacting case. This might be due to the mixing of the Hilbert space degrees of freedom for an interacting system. Moreover, adiabatic continuity demands that in the weakly interacting case, EE should also obey the sub-extensive law in the localized phase. Our macroscopic RG scheme might not be sufficient for studying this law which is deeply governed by the microscopic nature of the model. However, this outcome goes against the usual notion of localized phase in the context of MBL transition. We hence scrutinize our observation by considering the proper renormalized $W^* \gg W_c^*$. This restricts us to stay well inside the localized phase rather than in the vicinity of the crossover region. We there observe an absolute area law of EE in the finite size system that is depicted by violet dashed line in Fig. 3(b). Therefore, irrespective of the microscopic nature the renormalization of W again becomes relevant to observe the accurate behavior associated with a MBL phase (we discuss this at length in Sec. III B). We would like to emphasize that the deviation from the area law for $\alpha < 2$ is not an artifact of the RSRG scheme with nearest neighbour interaction. It rather might be intrinsically caused by the algebraic nature of the SPSS³⁸. As discussing the area law of MBL phase, it is also important to highlight a major difference between the mechanisms of thermalization for long-range models in comparison to the short-range models. In short range systems, a thermal inclusion thermalizes only spins in a fixed range depending on the localization length. Contrastingly, for long-range systems a such thermal inclusion will thermalize the whole systems. It means that delocalization is much more favorable for long-range models.

Turning to the Fig. 4(a), the visual inspection shows that the rescaling of disorder strength leads to an approximate coincidence of all rescaled curve up to a certain

point $W_c^* = 0.99$; $W^* > W_c^*$, the coincidence is lost and they start deviating from each other and S/L saturates to a higher value as L increases. Therefore, one can obtain a sharp transition point $W_c^* = 0.99$. Having obtained W_c^* , one can check the finite size exponent ν , following the data collapse technique near the transition point for $\alpha = 1.2$. Our focus would be obtain a proper collapse in the right side of W_c^* i.e., $W^* > W_c^*$ as the region $W^* < W_c^*$ is less of our interest. The functional form that we keep in our mind is $S/L = f((W^* - W_c^*)L^{1/\nu})$ near the transition point. We show in the inset of Fig. 4(a) that $(W - W_c^*)L^{1/\nu}$ plots of S/L for different L coincide (maximally for $W^* \geq W_c^*$) with each other near 0 with $\nu = 2.5 \pm 0.31$. To show the robustness of this exponent, we consider different interaction strength V and $\alpha < 2$. We find remarkably that critical exponent obtained for various settings are well inside the error bar.

On the other hand, we perform a data collapse for $\alpha = 2.5$ in Fig. 4(b) keeping the same mathematical form in our mind near the transition point: $S/L = f((W - W_c)L^{1/\nu})$. We note here that the renormalization of W is no longer required as the a sharp transition point is obtained from bare W unlike the case for $\alpha = 1.2$. Moreover, the localized phase obey area law for $W \gg W_c$. The interesting observation is that with $\nu = 3.1 \pm 0.25$, one can obtain a very nice data collapse around $W = W_c$ in both the sides.

Extraction of these exponents conveys a lot of physical message about the transition for $\alpha < 2$ and $\alpha > 2$. The transition observed for $\alpha = 2.5$ is qualitatively different from the one observed for $\alpha = 1.2$ as far as the critical exponents are concerned. However, the localized phases obtained for both sides of $\alpha = 2$ bear the signature of area law. The nature of data collapse we observe in Fig. 4(a) with $\alpha = 1.2$ allows us to convey the message that there might be two different critical exponents present in left and right side of W_c^* ³¹. By invoking the concept of correlation length ε in the Hilbert space of the problem near the transition point, we can write down the following scaling relation

$$\begin{aligned} \varepsilon(W^*) &\sim (W^* - W_c^*)^{-\nu_1}, & \text{for } W^* > W_c^*, \\ \varepsilon(W^*) &\sim (W_c^* - W^*)^{-\nu_2}, & \text{for } W^* < W_c^*. \end{aligned} \quad (3)$$

Here we consider $\nu_{1,2}$ being the correlation length exponent, when W_c^* is approached from above i.e., localized (below i.e., delocalized) phase. This is clearly not the case for $\alpha > 2$ as shown in Fig. 4(b) where a single exponent $\nu = 3.1$ can decisively collapse all S/L curves for different L .

The existence of two different ν in two sides of transition point might be related to the absence of proper length scale namely, localization length inside the system. Additionally, near the critical point in disordered system, there exists Griffiths phase⁶¹; this idea is also extensively explored in the context of MBL transition⁴⁹. One also needs to consider the effect of Griffiths phase in describing these exponents. However, what we would like to emphasize more is that for $\alpha < 2$, system essentially

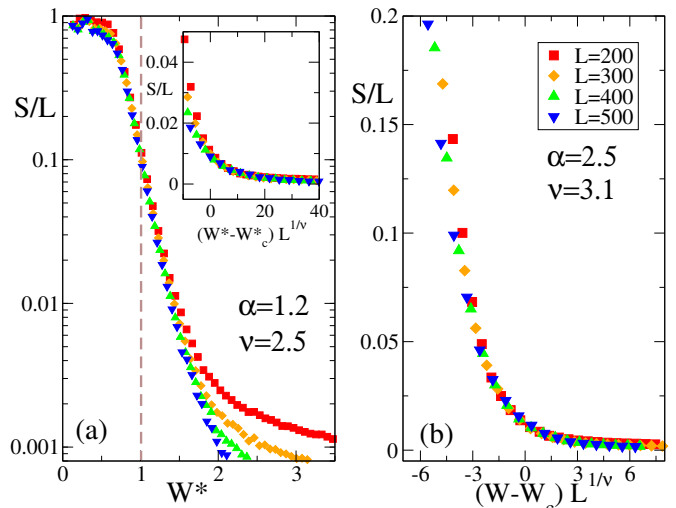


FIG. 4. (Color online) We here show the finite size scaling analysis for $\alpha = 1.2$ in (a) and $\alpha = 2.5$ in (b). (a): In order to identify a sharp transition point, we plot S/L as a function of rescaled disorder $W^* = W/\ln L$. The coincidence of S/L for different L is observed $W^* < W_c^* = 0.99$ after which S/L tends to deviate from each other and eventually saturates for $W^* \gg W_c^*$; this saturation value increases as L decreases. Inset shows a clear data collapse around 0 (maximally for $W^* > W_c^*$) when S/L is plotted as a function of $(W^* - W_c^*)L^{1/\nu}$ with $\nu = 2.5$. (b): We repeat the inset of (a) in (b) for $\alpha = 2.5$ considering the fact that $W_c = 3.95$. We find a perfect data collapse around 0 when S/L is plotted as a function of $(W - W_c)L^{1/\nu}$ with $\nu = 3.1$. These clearly suggests that the characteristics of transitions undergoing for $\alpha < 2$ and $\alpha > 2$ are qualitatively different.

being long range (we reiterate that SPSs of a microscopic long range Hamiltonian are algebraically localized)³⁴, the critical behavior associated with the MBL transition suggests that it belongs to a different universality class as compared to the MBL transition occurring for $\alpha > 2$. On the other hand, the MBL transition happening for $\alpha > 2$ belongs to the Anderson type universality class for short range system where SPSs are exponentially localized⁶⁰. We note that ν satisfies Harris criteria⁵⁶ for the MBL transition in both the sides of $\alpha = 2$. It is worth mentioning that the change in the universality class is also visited in the field of quantum spin chain where the range of spin-spin interaction is tuned⁶². It is indeed a strength of the RG analysis that even without considering a microscopic Hamiltonian, it can signal the change in the universality class while range of tunneling matrix element Γ_{ij} is varied.

We shall now investigate the behavior of normalized maximum block size (MBS) ξ/L . As stated above, MBS acquires the value of 1 in the delocalized phase while in the localized phase $\xi/L \rightarrow 0$. Let us begin by analyzing the Fig. 5(a) and Fig. 5(b) where ξ/L is shown for different L with $\alpha = 1.2$ and $\alpha = 2.5$, respectively. Findings suggest that delocalization ($\xi/L \sim 1$) to localization

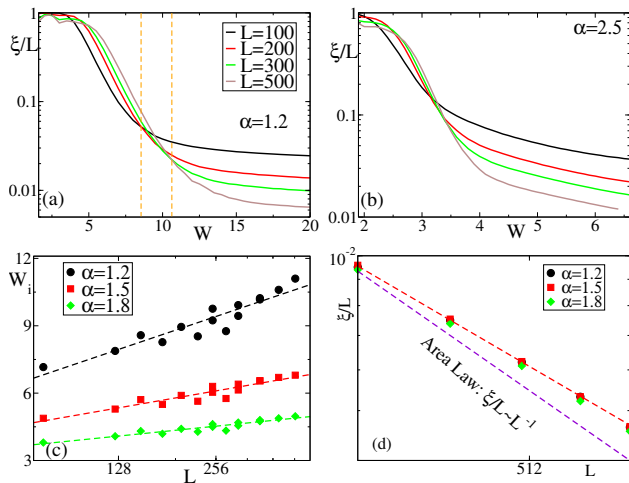


FIG. 5. (Color online) We here present the findings for maximum block size (MBS). (a): normalized MBS ξ/L shows a transition from high value (delocalized phase) to low value (localized phase), although, the intersection points shifts to higher values of W as one increases system size from $L = 100$ to 500. Here $\alpha = 1.2$. (b): We repeat (a) for $\alpha = 2.5$. Remarkably we find that there exists a sharp transition point $W_c = 3.3$ irrespective of the system size L . (c): We show the intersecting W_i follows similar logarithmic scaling with L (depicted by the best fit dashed lines) as obtained from EE: $W_i = \gamma \ln L$. γ reduces with increasing $\alpha < 2$. The solid red, black and green are numerical data points. (d): We show a scaling of ξ/L with L in a semi-log scale with $W = 20.0$ as depicted by solid red, black and green points. The area law is guaranteed in the localized phase for $W^* = 3.0$ as shown by the violet dashed line.

($\xi/L \ll 1$) crossover is undergoing for all values of L if we increase W sufficiently $W > \max\{W_i\}$. The intersection window ΔW appears a bit earlier than the one observed in EE for $\alpha = 1.2$. Figure 5(c) clearly indicates that W_i logarithmically scales with L . The crossover in the finite size system would corresponds to a proper transition phenomena if we renormalize W following the same scaling formula (2); similar to the case of EE, here also one can define a sharp transition point and data collapse. On the other hand, ξ/L shows a clear transition point at $W_c = 3.3$ for $\alpha = 2.5$ without any renormalization of disorder strength. Therefore, the qualitative differences between these two transitions occurring for $\alpha < 2$ (i.e., long range limit) and $\alpha > 2$ (i.e., short range limit) are also visible from MBS analysis. Lastly, Fig. 5(d) suggests that proper renormalization of W can guarantee the area law (depicted by violet dashed line) in the localized phase for $\alpha < 2$; the deviation from area law is an artifact of the finite size crossover phenomena.

We shall now make resort to an analytical formulation where one can qualitatively understand the crossover phenomena in the finite size system²⁹. Let us begin by considering a d -dimensional hypercube disordered long range model with N (equivalent to L) interacting spin-1/2 particle with spatial density n . Here two spins are

separated by R . Now the notion of the resonant pair comes in the picture when the system resides in a delocalized ergodic phase i.e., spins at different sites can club together and behave as a collective spin. In this phase, the probability to form a resonant pair is $P(R) \sim U_0/(WR^\alpha)$ where U_0 the energy scale spin-spin interaction and W is the disorder strength. The density of resonant pair of size R is then given by $n_p(R) \sim nR^d P(R) \sim nW^{-1}R^{-\alpha+d}$. Hence the total number of spin within a volume of R^d becomes $\tilde{N}(R) \sim nW^{-1}R^{-\alpha+2d}$. The effective average distance is given by $n_p^{-1/d}$. The effective interaction within this average distance then takes the form

$$V(R) \sim \frac{1}{(n_p^{-1/d})^\alpha} \sim W^{-\frac{\alpha}{d}} R^{\frac{\alpha(-\alpha+d)}{d}} \sim W^{-\frac{\alpha}{d}} \left[\frac{1}{R^d} \right]^{\frac{\alpha(\alpha-d)}{d^2}}. \quad (4)$$

On the other hand, the characteristic energy of such pair given by

$$E(R) \sim R^{-\alpha} \sim \frac{1}{(R^d)^{\frac{\alpha}{d}}}. \quad (5)$$

Therefore, combining these two energy scales in Eq. (4) and Eq. (5), one can infer that the resonance can only proliferate if effective interaction exceeds the characteristic energy. The condition we obtain then

$$\frac{\alpha(\alpha-d)}{d^2} < \frac{\alpha}{d}. \quad (6)$$

This can be simplified as $\alpha < 2d$. One can thus argue that delocalization can take place for sufficiently large system $L \gg R$ when $\alpha < 2d$. In the above argument we concentrate only on the exponent associated with R and subside the influence of disorder strength W . Therefore, the limit of large L limit requires proper scaling of W with the system size. What we mean by that is the following: for a given disorder strength W , tendency towards delocalization increases with L and, equivalently, for a given system size L , tendency towards localization increases with increasing W . Therefore, critical length $L_c(W)$ or critical disorder $W_c(L)$ both can exist. The above line of argument further suggests that if the system size becomes comparable with the size of the resonant pair $L \simeq R$ and $\tilde{N}(L) \sim 1$: one can obtain $W_c(L) \sim L^{(2d-\alpha)/\alpha}$ and similarly, $L_c(W) \sim W^{\alpha/(2d-\alpha)}$. Hence, interestingly, for finite L true localization transition happens to be a crossover. Moreover, for $\alpha < 2d$, $\tilde{N}(L)$ ranges from very small value to large value as L varies from very small value to large value referring to the fact that many-body delocalization transition is taking place. If thermodynamics limit is taken by considering W and L both simultaneously to infinity keeping $W/W_c(L)$ fixed, one obtains localized phase for $W > W_c(L)$ and delocalized phase for $W < W_c(L)$. One can connect it to phase diagram obtained in $W - L$ plain as represented in Ref.³¹.

Now the interesting question is how much it is true that W_c follows an algebraic scaling with L . The resonances occurring inside the system are not of very simple type rather the emerging network of the many-body

states coupled by these resonances has a treelike structure. To be precise, resonant structure in the many-body Hilbert space can be viewed as a random regular graph^{30,31,63}. Moreover, the resonances can be identified distinctly from those encountered on the previous step resulting in an emergence of spectral diffusion factor⁶⁴. Under these circumstances, lattice with connectivity $K \gg 1$, the critical value of disorder enhanced by a factor of $\ln K$. Generally, for a lattice of size L , $K = f(L)$. Hence, W_c should contain a logarithmic and an algebraic factor dependent on L . However, in this present case, we find W_c scales as logarithmically. This could be an artifact of finite size limitation. As we know, in the large L limit $\ln L$ can be suppressed by the algebraic factor while in the small L limit, $\ln L$ would be predominant over the algebraic factor. We additionally note that in our case of nearest neighbour short range interaction might not be able to capture the accurate scaling of critical disorder with finite size of the system; furthermore, long range interaction might enhance localization and lower the critical disorder as compared to the short range interaction^{32,58}. The MBL phase is found to be destabilized once the long range interaction decays slower than exponentially⁵⁹. We would like to reiterate that in the thermodynamic limit $L \rightarrow \infty$, MBL phase for $\alpha > 2$, obtained following macroscopic RSRG scheme, might suffer from instability. The algebraic nature of the coupling i.e., algebraic localization can cause this instability. However, from numerical ED study it is not very conclusive that what is the effect of long range interaction on MBL transition⁶⁵.

B. Microscopic RG

Even though, we believe our previous RSRG scheme in Sec. III A is able to capture the main essence of the long-range models. In this section, we again do similar studies but now incorporate the microscopic details of a particular long-range Hamiltonian in the RSRG Scheme. Specially, using the microscopic RG scheme, the role of instability of MBL for $\alpha > 2$ can be probed more extensively even with finite size of system $L \sim O(10^2)$. The specific long-range microscopic model, we use to modify the RG scheme is described by the following Hamiltonian,

$$H = - \sum_{i,j \neq i} \frac{J_{i,j}}{(1 + |i-j|^{2\alpha})^{1/2}} (\hat{c}_i^\dagger \hat{c}_j + \text{H.c.}) + \sum_i \mu_i \hat{n}_i \quad (7)$$

where \hat{c}_i^\dagger (\hat{c}_i) is the fermionic creation (annihilation) operator at site i , $\hat{n}_i = \hat{c}_i^\dagger \hat{c}_i$ is the number operator, and L is the size of the system. J_{ij} and μ_i are uniform random number chosen from an interval $[-1, 1]$ and $[-W, W]$ respectively. For $\alpha > 1$ the single particle states of this Hamiltonian are algebraically localized. We first carry out ED calculation of this non-interacting Hamiltonian and obtain all single particle energies and eigen-

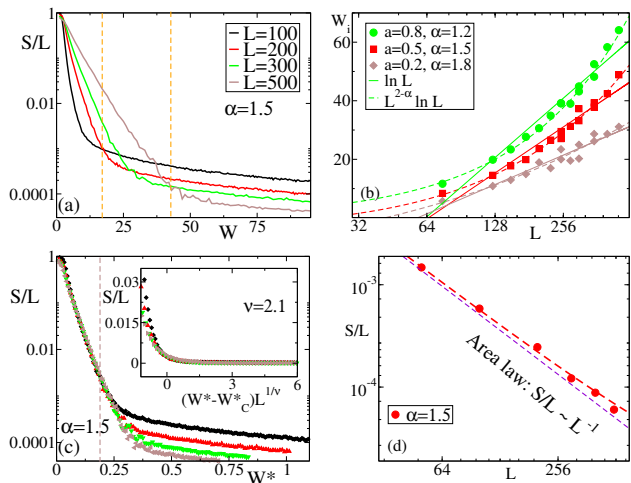


FIG. 6. (Color online) We here present the findings of EE putting the microscopic detail of the Hamiltonian (7) in our RG scheme. (a) EE density S/L decreases from 1 with increasing the disorder strength W for $L = 100, 200, 300$, and 500 . Here $\alpha = 1.2$. The intersection points of S/L curve between different values of L , shifts to higher values of W as one increases system size. (b): Intersection points obtained from (a), depicted by solid red, green and brown points, scales with system size as $L^{2-\alpha} \ln L$ that is represented by the dashed lines. The logarithmic fitting $\ln L$ as depicted by solid lines are not in good agreement with the numerical data points, specifically, for $\alpha = 1.2$ and 1.5 . (c) We again show the variation of S/L with rescaled disorder strength $W^* = W/L^{2-\alpha} \ln L$. We identify the transition point as $W_c^* = 0.19$. In the inset, we show data collapse $S/L = f((W^* - W_c^*)L^{1/\nu})$ for $\nu = 2.25$ and for $W^* > W_c^*$. (d): We show a scaling of S/L with L in a log-log scale with $W = 80.0$ as depicted by solid red points. The area law is guaranteed for $W^* = 1.0$ in the localized phase as depicted by the dashed violet line.

states. Given that a typical single-particle eigenstate with eigenenergy ϵ_i is of the form $\psi_i \sim 1/|i - r_0|^\alpha$, where $r_0 \neq i$ is the localization center. We now initialize our RG scheme by defining $\Delta E_{ij} = |\epsilon_i - \epsilon_j|$ i.e., the difference between the eigenenergies of the Hamiltonian (7). We consider $\Gamma_{ij} = 1/|i_0 - j_0|^\alpha$ where i_0, j_0 are the localization center correspond to the i -th and j -th eigenstate of the Hamiltonian. We note that the interacting version of this model has been studied where the MBL phase is characterized by the algebraically decaying tails of an extensive number of integrals of motion, unlike the case of exponentially localized SPSS⁶⁶.

In Fig. 6(a), we show the variation entanglement density as function of W for different values of L . Similar to the outcome from macroscopic scheme, the intersection point W_i shifts to higher value with increasing L ; we note that the window ΔW and the values of W_i both acquire higher values compared to the earlier case. In order to search for the sharp transition point, we then try to estimate the proper scaling law of W_i with L in Fig. 6(b) for $\alpha = 1.2, 1.5$ and 1.8 . Interestingly, the microscopic in-

put modifies the scaling function; it becomes more rapid compared to the slow $\ln L$ scaling as shown in Eq.(2):

$$W^* = \frac{W}{L^{2-\alpha} \ln L}. \quad (8)$$

This form of renormalization confirms the predicted scaling by Mirlin et al.³¹ following an ED scheme in interacting spin model where hopping and interaction both considered to be long range. Even though, the microscopic input that we use here is from a long-range non-interacting model (7), but our RSRG scheme does not incorporate long-range interaction. Interestingly, we still manage to mimic the underlying physics of the long range model unambiguously irrespective of the range of interaction⁶⁵. The scaling form (8) also matches well with the analytical prediction in the context of random regular graph³⁰ that we discussed in Sec. (III A). Hence, microscopic detail in RG scheme helps in obtaining more accurate behavior for the observables. We further check that logarithmic scaling $W_i \sim \ln L$ (as depicted by solid lines in Fig. 6 (b)) is not the accurate renormalization of W_i for the microscopic RG scheme. Here, the algebraic scaling form prevails referring to the fact that finite size effect is relatively minimized compared to macroscopic RG scheme.

A very recent ED study shows that long-range interaction is not able to influence the thermal-MBL transition property of the system in a noticeable manner⁶⁵. Contrastingly, MBL might persist in the presence of long-range interactions though long-range hopping with $1 < \alpha < 2$ delocalizes the system partially, while almost all the states are extended for $\alpha \leq 1$. On the other hand, our study of microscopic RSRG study with short range diagonal interaction indicates the fact that critical disordering follow similar scaling with L as observed in long-range interacting system.

Similar to the Fig. 4(a), the EE density for different L coincide with each other when $W^* < W_c^* = 0.33$, after that they start deviating from each other for $W^* \geq W_c^*$. For $W^* \gg W_c^*$, the saturation values of EE density increases with decreasing L . Comparing Fig. 4(a) and Fig. 6(c), one can see that the tendency towards saturation is more once the RSRG scheme is embedded with the microscopic detail. Now we shall investigate the scaling form of $S/L = f((W^* - W_c^*)L^{1/\nu})$ from the data collapse analysis as shown in Fig. 6(c). We show here that with $\nu = 2.25 \pm 0.3$, one can obtain a nice data collapse for $W^* \geq W_c^*$. We also checked the critical properties for $\alpha = 2.5$ where we find exponent $\nu = 2.9 \pm 0.27$. Hence, these values of the critical exponent are well corroborated to their counterpart obtained from macroscopic RSRG approach satisfying the Harris criterion⁵⁶. Therefore, microscopic RG reconfirms that the universality class for $\alpha < 2$ is different than that of the for $\alpha > 2$. Finally, in Fig. 6(d), we show that the area law (violet dashed line) is recovered for localized phase in the the regime $W^* \gg W_c^*$.

We now show the variation of S/L with W for $\alpha = 2.5$

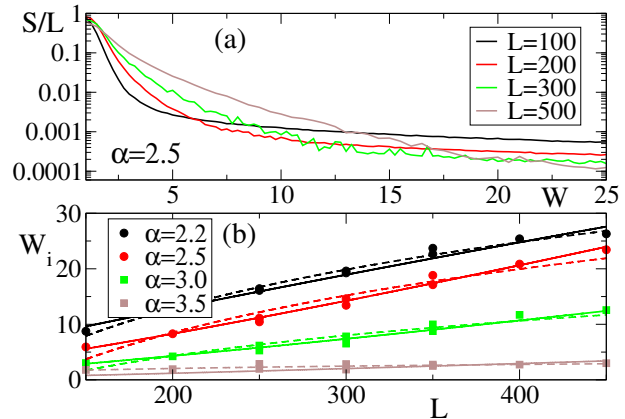


FIG. 7. (Color online) The behavior of EE density as a function of disorder strength W is shown for microscopic RSRG scheme for $\alpha = 2.5$ in (a). It clearly suggests that there is finite delocalization-localization cross-over window in $W\{W_i\}$ for $\alpha = 2.5$. We then try to estimate the behavior of W_i with the system size L considering two fitting function $m \ln L + n$ (dashed lines) and $p \exp(q \sqrt{\ln L})$ (solid lines) as shown in (b). One can observe that for α being well above 2, $p \exp(q \sqrt{\ln L})$ yields apparently better fit compared to $m \ln L + n$. We find $m = 17.2, 16.5, 9.1, 1.0$, and $n = -78.3, -79.2, -43.9, -3.5$ for $\alpha = 2.2, 2.5, 3.0, 3.5$, respectively. We find $p = 4.0 \times 10^{-4}, 4.8 \times 10^{-6}, 2.5 \times 10^{-6}, 0.9 \times 10^{-7}$ and $q = 4.5, 6.2, 6.1, 6.0$ for $\alpha = 2.2, 2.5, 3.0, 3.5$, respectively.

using the microscopic RSRG approach in Fig. 7. Unlike the case of the macroscopic RSRG scheme, here we find that W_c increases with L even for $\alpha > 2$. However, the scaling of W_c with L becomes much slower compared to the one obtained before for $\alpha < 2$. Figure. 7 shows the variation of W_c with L for $\alpha = 2.2, 2.5, 3.0$, and 3.5 . We find almost equally good agreement by fitting our results with two functional forms 1) $\sim \ln L$ and 2) $\sim \exp(\text{const} \sqrt{\ln L})$. The later one has been predicted in Ref.^{58,63} for $\alpha > 2$ in presence of long-range interactions.

IV. COMPARISON BETWEEN MICROSCOPIC AND MACROSCOPIC RSRG

In this section, we compare between two RSRG schemes which we have used in this work. Even though, both RSRG approaches conclude the critical disorder strength W_c is an increasing function of L , the finite size scaling of W_c are not very different in two approaches at least for $\alpha < 2$. While the microscopic RSRG predicts $W_c(L) \sim L^{2-\alpha} \ln L$, the macroscopic RSRG predicts $W_c(L) \sim L^\eta \ln L$ with $\eta \ll 2 - \alpha$ for $\alpha < 2$. We believe that one of the main reason behind this discrepancy is due to the difference between the spacing distribution of the on-site energies in two approaches. In

the microscopic RSRG scheme, the initial on-site energies have been taken from a uniform random distribution and hence, spacing distribution is Poissonian. On the other hand, in the microscopic RSRG approach, the on-site energies are taken from the eigenvalues of the microscopic Hamiltonian (7), the spacing distribution of eigen-energies of the Hamiltonian (7) are not exactly Poissonian⁶⁷, they show the signature of level-repulsion at least for $\alpha < 2$. Hence, the microscopic RSRG scheme promotes avalanche mechanism^{58,59}. This is presumably the reason the scaling $W_c(L)$ with L is much faster in this scheme compared to macroscopic RSRG scheme.

Now we investigate the distribution of the normalized MBS ξ/L for both RSRG schemes and for $\alpha = 1.5$ and 2.5. We show our results for 4 different values of quenched disorder of strength W in Fig. 8. One value of W is chosen such that $W \ll W_c(L)$ (denoted with black points in the Fig. 8), for which the peak of the distribution is at $\xi/L \simeq 1$ signifying complete delocalization. Another value of W is chosen such that $W \gg W_c(L)$ (denoted with blue points in the Fig. 8), for which the peak of the distribution is at $\xi/L \ll 1$ and that signifies complete localization. On the other hand, we also show the results for two other values of W , which are taken from the vicinity of W_c (denoted with red and green points in the Fig. 8). The MBS distribution shows bi-modal distribution having two peaks one at $\xi/L \simeq 1$ and another at $\xi/L \ll 1$. The presence of cluster with MBS $\simeq L$ in this regime might refer to the instability of phase transition; the system flows towards the thermalizing phase due to its inbuilt avalanche mechanism.

There is no significant qualitative differences between the distribution of MBS in two RG approaches. However, the inset plots of S/L vs W suggest (insets of Fig. 8) that within the microscopic RSRG approach the plateau region of EE for $W \ll W_c$ is absent (S/L starts decreasing as soon as W is increased) in comparison to the macroscopic RSRG scheme. This leads to a few quantitative differences while the distribution of MBS is studied. The height of the peak of MBS distribution at $\xi/L \sim 1$ for $W \ll W_c$ is much less ($C \sim 0.5$) for the microscopic RSRG compared to the macroscopic RSRG scheme ($C \sim 1$). In particular, for delocalized phase observed following microscopic RG, histogram of MBS C gets distributed over a range $0.5 \leq \xi/L \leq 1.0$ which is not observed for macroscopic RG. On the other hand, the disorder window of cross-over region showing the bi-modal distribution becomes shortened for macroscopic RG compared to microscopic RG. This enhancement in the cross-over window for microscopic RG again refers to the fact that W_c-L scaling can differ.

We now show the behavior of the cross-over window $\Delta W = W_i(L_{\max}) - W_i(L_{\min})$ as a function of α for macroscopic RG and microscopic RSRG scheme in Fig. 9 (a) and (b), respectively, where L_{\max} and L_{\min} are the largest and the smallest system sizes used for our numerical calculations. It is evident from the plot ΔW vs. α for macroscopic RSRG, ΔW is significantly small for $\alpha > 2$

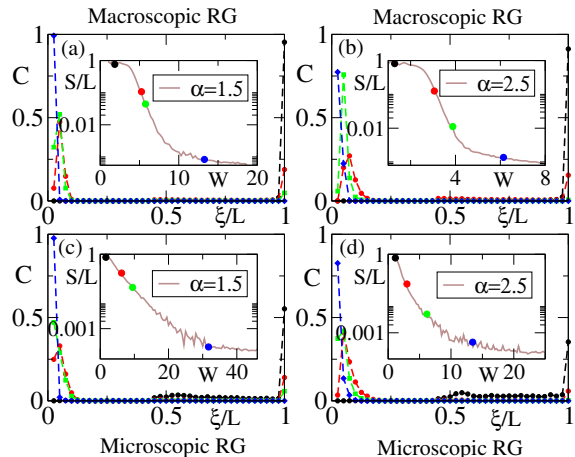


FIG. 8. (Color online) We investigate the histogram of normalized MBS C as a function of ξ/L for microscopic RSRG with $\alpha = 1.5$ (a), $\alpha = 2.5$ (b) and macroscopic RSRG with $\alpha = 1.5$ (c), $\alpha = 2.5$ (d). We choose four representative points as marked by black, red, green, blue solid circles in inset where EE density is plotted with W for $L = 300$. We show the variation of histogram count C as a function of ξ/L for the above four representative points with specified W . One can clearly observe from both of the RSRG scheme that the distribution pattern changes from uni-modal (when system remains deep inside localized/ delocalized phase) to bi-modal (when the system in the vicinity of delocalization-localization cross-over window). For $\alpha = 2.5$, disorder window of W within which bi-modal distribution appears, gets reduced compared to $\alpha = 1.5$.

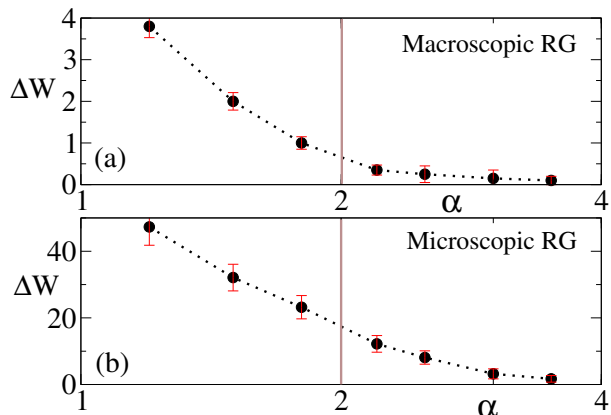


FIG. 9. (Color online) We plot the crossover window in disorder ΔW , with α obtained from macroscopic RG and microscopic RG in (a) and (b), respectively. We here use $L = 100, \dots, 500$ data to estimate ΔW . The distinct behavior is observed around $\alpha = 2$ at least for (a).

compared to $\alpha < 2$. Hence, it is almost impossible to find finite size scaling of W_i in this parameter regime. On the other hand, within microscopic RSRG scheme ΔW remains relatively large even for $\alpha > 2$, hence, it has been possible to study the system size dependence of $W_c(L)$ in this parameter regime, which seems to satisfy the following scaling function: $W_c(L) \sim \exp(\text{const}\sqrt{\ln L})$. In addition, we also note that area law of EE is satisfied for $\alpha > 2$ for both of the cases without rescaling the disorder strength. Therefore, there are some qualitative changes occurring around $\alpha = 2$ which need to be addressed more extensively in future.

We also like to emphasize that even within macroscopic RSRG approach ΔW for $\alpha \geq 2$, is not strictly zero even for our choice of system sizes as shown in Fig. 9 (a). However, the variation of W_i with L within macroscopic RSRG approach is very small, when $L \in [50, 500]$. Hence one does not even need to re-scale W with appropriate L dependent scaling functions to see delocalization-MBL transition (as shown in Fig. 2 (b)). This does not necessarily mean that MBL phase is stable in the thermodynamic limit. There is always a possibility that if we could manage to do our calculations for significant large system sizes compared to what we have presented here, we might obtain ΔW large enough to find system size dependence scaling function for W_c . Strikingly, in the microscopic RSRG approach even for $L \in [50, 500]$, we find ΔW to be large enough to extract a L dependent scaling function for W_c , which proves the instability of MBL phase in these models in the thermodynamic limit.

V. CONCLUSION

In this work, we propose a new RSRG scheme to investigate thermal-MBL transition in a one-dimensional long-range models with hopping $t \sim r^{-\alpha}$, where SPSs are algebraically localized with localization exponent $\alpha > 1$. Within this approach, in presence of nearest neighbour interaction, we show that indeed there is a crossover between delocalized and localized phase as a function of quenched disorder W for $\alpha < 2$. In last few years, there have been several studies leading to conflicting claims about the true nature of this transition^{29,65}. Most of those studies involve ED that is restricted within small system size. Our RSRG approach allows us to extend system size up to $L \simeq 500$, with which we can investigate the finite size scaling of transition points systematically. Even though this scaling appears to be dependent on RG scheme, the most realistic implementation of RG rules predicts the scaling to be $\sim L^{2-\alpha} \ln L$. This form supports the prediction of Ref.³¹. We hence propose that one can still talk about thermal-MBL transition in appropriate thermodynamic limit as function of rescaled quenched disorder $W^* = W/L^{2-\alpha} \ln L$. Moreover, the apparent deviation from the area law in the MBL phase is also remarkably resolved upon considering W^* . Most

interestingly, with this non-trivial rescaling for $\alpha < 2$, we obtain different correlation length exponents associated with the transition which is qualitatively and quantitatively different from a usual MBL transition observed in short range system. On the contrary, the MBL transition for $\alpha > 2$ requires no rescaling of W and surprisingly, it belongs to the same Anderson type universality class for the short range systems.

A recent study claims the range of interactions does not influence the thermal-MBL transitions as long as long-range hopping is present in the systems⁶⁵. The finite size scaling of the critical disorder strength obtained from our calculations matches with analytical prediction for long-range interacting models^{31,58}. Our findings qualitatively supplement ED results along with the possibility that $\alpha = 2$ can be a special point. However, for long-range hopping system without diagonal interaction, the MBL transition might occur for $a > 3/2$ ⁶⁸; with diagonal interaction the crossover point $a = 3/2$ is not found to be conclusive²². Combining all these above discussions, we can infer that the location of the exact crossover point for short range diagonal interaction (long-range hopping) is a subject of further study.

One can note that the apparent dissimilarity in the scaling of critical disorder for macroscopic and microscopic RSRG, might be caused by the average level spacing statistics of the initial input energies of these model e.g., macroscopic RSRG supports Poissonian distribution while for microscopic RSRG it deviates towards Wigner-Dyson distribution. This promotes the avalanche mechanism^{58,59} in the system, and destabilizes the MBL phase faster. In this context of stability of MBL phase for short range system, it is also important to mention the recent studies. These suggest that in order to observe a MBL transition, one needs to consider thermodynamically large systems supporting Thouless time scale comparable to Heisenberg time scale^{28,69-71}. We believe that it would be interesting to investigate these time scales for long-range systems as well.

The statistics of many-body energy levels of long-range systems is experimentally investigated in superconducting circuit⁷² and trapped ion⁷³⁻⁷⁵. On the other hand, long range hopping is also realized in laboratory^{42,44}. We therefore believe that our findings can be experimentally testable in near future. One natural extension to our work would be to analyze the effect of long range interaction and probe the MBL transition which has already been investigated using self-consistent theory and ED^{32,76}. An sub-extensive law of EE in the localized phase is clearly observed for non-interacting system³⁸; then the question becomes in presence of interaction is this law suppressed and EE tends toward the area law. Hence, a possible future direction would be to critically analyze the scaling of EE in a thermodynamically large system with various other RSRG scheme incorporating appropriate microscopic detail. On the other hand, the existence of Floquet time crystal in this long range model can be another field of research.

VI. ACKNOWLEDGEMENT

We would like to thank Andrew C. Potter for initial discussion regarding the RSRG algorithm. We also thank

Anirban Roy for helping us with some relevant python packages during our numerical calculation.

-
- ¹ D. Basko, I. Aleiner, and B. Altshuler, *Annals of physics* **321**, 1126 (2006).
- ² A. Pal and D. A. Huse, *Physical Review B* **82**, 174411 (2010).
- ³ P. W. Anderson, *Physical review* **109**, 1492 (1958).
- ⁴ L. Fleishman and P. W. Anderson, *Phys. Rev. B* **21**, 2366 (1980).
- ⁵ B. L. Altshuler, Y. Gefen, A. Kamenev, and L. S. Levitov, *Phys. Rev. Lett.* **78**, 2803 (1997).
- ⁶ S. Gopalakrishnan, M. Müller, V. Khemani, M. Knap, E. Demler, and D. A. Huse, *Phys. Rev. B* **92**, 104202 (2015).
- ⁷ V. Khemani, R. Nandkishore, and S. L. Sondhi, *Nat. Phys.* **11**, 560565 (2015).
- ⁸ J. H. Bardarson, F. Pollmann, and J. E. Moore, *Physical review letters* **109**, 017202 (2012).
- ⁹ V. Khemani, S. P. Lim, D. N. Sheng, and D. A. Huse, *Phys. Rev. X* **7**, 021013 (2017).
- ¹⁰ M. Žnidarič, T. c. v. Prosen, and P. Prelovšek, *Phys. Rev. B* **77**, 064426 (2008).
- ¹¹ D. Pekker, G. Refael, E. Altman, E. Demler, and V. Oganesyan, *Phys. Rev. X* **4**, 011052 (2014).
- ¹² M. Rigol, V. Dunjko, V. Yurovsky, and M. Olshanii, *Phys. Rev. Lett.* **98**, 050405 (2007).
- ¹³ M. Rigol, V. Dunjko, and M. Olshanii, *Nature* **452**, 854 (2008).
- ¹⁴ L. F. Santos and M. Rigol, *Phys. Rev. E* **81**, 036206 (2010).
- ¹⁵ M. Rigol, *Phys. Rev. Lett.* **103**, 100403 (2009).
- ¹⁶ L. Vidmar and M. Rigol, *J. Stat. Mech.* **2016**, 064007 (2016).
- ¹⁷ G. De Chiara, S. Montangero, P. Calabrese, and R. Fazio, *Journal of Statistical Mechanics: Theory and Experiment* **2006**, P03001 (2006).
- ¹⁸ M. Fagotti, P. Calabrese, and J. E. Moore, *Physical Review B* **83**, 045110 (2011).
- ¹⁹ V. Khemani, A. Lazarides, R. Moessner, and S. L. Sondhi, *Phys. Rev. Lett.* **116**, 250401 (2016).
- ²⁰ D. V. Else, B. Bauer, and C. Nayak, *Phys. Rev. Lett.* **117**, 090402 (2016).
- ²¹ M. Serbyn, M. Knap, S. Gopalakrishnan, Z. Papić, N. Y. Yao, C. R. Laumann, D. A. Abanin, M. D. Lukin, and E. A. Demler, *Phys. Rev. Lett.* **113**, 147204 (2014).
- ²² N. Y. Yao, C. R. Laumann, S. Gopalakrishnan, M. Knap, M. Müller, E. A. Demler, and M. D. Lukin, *Phys. Rev. Lett.* **113**, 243002 (2014).
- ²³ M. Schreiber, S. S. Hodgman, P. Bordia, H. P. Lüschen, M. H. Fischer, R. Vosk, E. Altman, U. Schneider, and I. Bloch, *Science* **349**, 842 (2015).
- ²⁴ J.-y. Choi, S. Hild, J. Zeiher, P. Schauß, A. Rubio-Abadal, T. Yefsah, V. Khemani, D. A. Huse, I. Bloch, and C. Gross, *Science* **352**, 1547 (2016).
- ²⁵ M. Serbyn, Z. Papić, and D. A. Abanin, *Physical review letters* **110**, 260601 (2013).
- ²⁶ V. Ros, M. Müller, and A. Scardicchio, *Nuclear Physics B* **891**, 420 (2015).
- ²⁷ M. Žnidarič and M. Ljubotina, *Proceedings of the National Academy of Sciences* **115**, 4595 (2018).
- ²⁸ J. Šuntajs, J. Bonča, T. Prosen, and L. Vidmar, *arXiv preprint arXiv:1905.06345* (2019).
- ²⁹ A. L. Burin, *Phys. Rev. B* **91**, 094202 (2015).
- ³⁰ D. B. Gutman, I. V. Protopopov, A. L. Burin, I. V. Gornyi, R. A. Santos, and A. D. Mirlin, *Phys. Rev. B* **93**, 245427 (2016).
- ³¹ K. S. Tikhonov and A. D. Mirlin, *Phys. Rev. B* **97**, 214205 (2018).
- ³² S. Roy and D. E. Logan, *SciPost Phys.* **7**, 42 (2019).
- ³³ P. Hauke and M. Heyl, *Phys. Rev. B* **92**, 134204 (2015).
- ³⁴ X. Deng, V. E. Kravtsov, G. V. Shlyapnikov, and L. Santos, *Phys. Rev. Lett.* **120**, 110602 (2018).
- ³⁵ X. Deng, S. Ray, S. Sinha, G. Shlyapnikov, and L. Santos, *arXiv preprint arXiv:1808.03585* (2018).
- ³⁶ M. Saha, S. K. Maiti, and A. Purkayastha, *arXiv preprint arXiv:1907.08536* (2019).
- ³⁷ M. Saha, A. Purkayastha, and S. K. Maiti, *arXiv preprint arXiv:1905.06644* (2019).
- ³⁸ R. Modak and T. Nag, *arXiv preprint arXiv:1903.05099* (2019).
- ³⁹ S. Pappalardi, A. Russomanno, B. Žunkovič, F. Iemini, A. Silva, and R. Fazio, *Phys. Rev. B* **98**, 134303 (2018).
- ⁴⁰ A. Leroze, B. Žunkovič, A. Silva, and A. Gambassi, *Phys. Rev. B* **99**, 121112 (2019).
- ⁴¹ A. Leroze, B. Žunkovič, J. Marino, A. Gambassi, and A. Silva, *Phys. Rev. B* **99**, 045128 (2019).
- ⁴² L. Childress, M. G. Dutt, J. Taylor, A. Zibrov, F. Jelezko, J. Wrachtrup, P. Hemmer, and M. Lukin, *Science* **314**, 281 (2006).
- ⁴³ M. G. Dutt, L. Childress, L. Jiang, E. Togan, J. Maze, F. Jelezko, A. Zibrov, P. Hemmer, and M. Lukin, *Science* **316**, 1312 (2007).
- ⁴⁴ K.-K. Ni, S. Ospelkaus, M. H. G. de Miranda, A. Pe'er, B. Neyenhuis, J. J. Zirbel, S. Kotochigova, P. S. Julienne, D. S. Jin, and J. Ye, *Science* **322**, 231 (2008).
- ⁴⁵ M. H. G. de Miranda, A. Chotia, B. Neyenhuis, D. Wang, G. Quemener, S. Ospelkaus, J. L. Bohn, J. Ye, and D. S. Jin, *Nat. Phys.* **7**, 502 (2011).
- ⁴⁶ S. Korenblit, D. Kafri, W. C. Campbell, R. Islam, E. E. Edwards, Z.-X. Gong, G.-D. Lin, L.-M. Duan, J. Kim, K. Kim, *et al.*, *New Journal of Physics* **14**, 095024 (2012).
- ⁴⁷ J. Sous and E. R. Grant, *New Journal of Physics* (2018).
- ⁴⁸ J. Sous and E. Grant, *Physical review letters* **120**, 110601 (2018).
- ⁴⁹ R. Vosk, D. A. Huse, and E. Altman, *Phys. Rev. X* **5**, 031032 (2015).
- ⁵⁰ A. C. Potter, R. Vasseur, and S. A. Parameswaran, *Phys. Rev. X* **5**, 031033 (2015).
- ⁵¹ L. Zhang, B. Zhao, T. Devakul, and D. A. Huse, *Phys. Rev. B* **93**, 224201 (2016).
- ⁵² A. Morningstar and D. A. Huse, *Phys. Rev. B* **99**, 224205 (2019).

- ⁵³ A. Goremykina, R. Vasseur, and M. Serbyn, *Phys. Rev. Lett.* **122**, 040601 (2019).
- ⁵⁴ P. T. Dumitrescu, R. Vasseur, and A. C. Potter, *Phys. Rev. Lett.* **119**, 110604 (2017).
- ⁵⁵ S.-X. Zhang and H. Yao, *Phys. Rev. Lett.* **121**, 206601 (2018de to).
- ⁵⁶ A. B. Harris, *Journal of Physics C: Solid State Physics* **7**, 1671 (1974).
- ⁵⁷ J. T. Chayes, L. Chayes, D. S. Fisher, and T. Spencer, *Phys. Rev. Lett.* **57**, 2999 (1986).
- ⁵⁸ S. Gopalakrishnan and D. A. Huse, *Phys. Rev. B* **99**, 134305 (2019).
- ⁵⁹ W. De Roeck and F. Huveneers, *Phys. Rev. B* **95**, 155129 (2017).
- ⁶⁰ D. J. Luitz, N. Laflorencie, and F. Alet, *Phys. Rev. B* **91**, 081103 (2015).
- ⁶¹ R. B. Griffiths, *Phys. Rev. Lett.* **23**, 17 (1969).
- ⁶² A. Dutta and J. K. Bhattacharjee, *Phys. Rev. B* **64**, 184106 (2001).
- ⁶³ K. S. Tikhonov, A. D. Mirlin, and M. A. Skvortsov, *Phys. Rev. B* **94**, 220203 (2016).
- ⁶⁴ I. Gornyi, A. Mirlin, D. Polyakov, and A. Burin, *Ann. Phys.* **529**, 1600360 (2017).
- ⁶⁵ S. Nag and A. Garg, *Phys. Rev. B* **99**, 224203 (2019).
- ⁶⁶ G. De Tomasi, *Phys. Rev. B* **99**, 054204 (2019).
- ⁶⁷ P. A. Nosov, I. M. Khaymovich, and V. E. Kravtsov, *Phys. Rev. B* **99**, 104203 (2019).
- ⁶⁸ A. O. Maksymov and A. L. Burin, *Phys. Rev. B* **101**, 024201 (2020).
- ⁶⁹ D. A. Abanin, J. H. Bardarson, G. D. Tomasi, S. Gopalakrishnan, V. Khemani, S. A. Parameswaran, F. Pollmann, A. C. Potter, M. Serbyn, and R. Vasseur, arXiv:1911.04501 (2019).
- ⁷⁰ J. Z. P. Sierant, D. Delande, arXiv:1911.06221 (2019).
- ⁷¹ R. K. Panda, A. Scardicchio, M. Schulz, S. R. Taylor, and M. Žnidarič, *EPL (Europhysics Letters)* **128**, 67003 (2020).
- ⁷² P. Roushan, C. Neill, J. Tangpanitanon, V. M. Bastidas, A. Megrant, R. Barends, Y. Chen, Z. Chen, B. Chiaro, A. Dunsworth, A. Fowler, B. Foxen, M. Giustina, E. Jeffrey, J. Kelly, E. Lucero, J. Mutus, M. Neeley, C. Quintana, D. Sank, A. Vainsencher, J. Wenner, T. White, H. Neven, D. G. Angelakis, and J. Martinis, *Science* **358**, 1175 (2017).
- ⁷³ H. Häffner, W. Hänsel, C. Roos, J. Benhelm, M. Chwalla, T. Körber, U. Rapol, M. Riebe, P. Schmidt, C. Becher, *et al.*, *Nature* **438**, 643 (2005).
- ⁷⁴ J. Zhang, G. Pagano, P. W. Hess, A. Kyprianidis, P. Becker, H. Kaplan, A. V. Gorshkov, Z.-X. Gong, and C. Monroe, *Nature* **551**, 601 (2017).
- ⁷⁵ H. Bernien, S. Schwartz, A. Keesling, H. Levine, A. Omran, H. Pichler, S. Choi, A. S. Zibrov, M. Endres, M. Greiner, *et al.*, *Nature* **551**, 579 (2017).
- ⁷⁶ P. Sierant, K. Biedro, G. Morigi, and J. Zakrzewski, *SciPost Phys.* **7**, 8 (2019).